Faraday Discussions

Accepted Manuscript

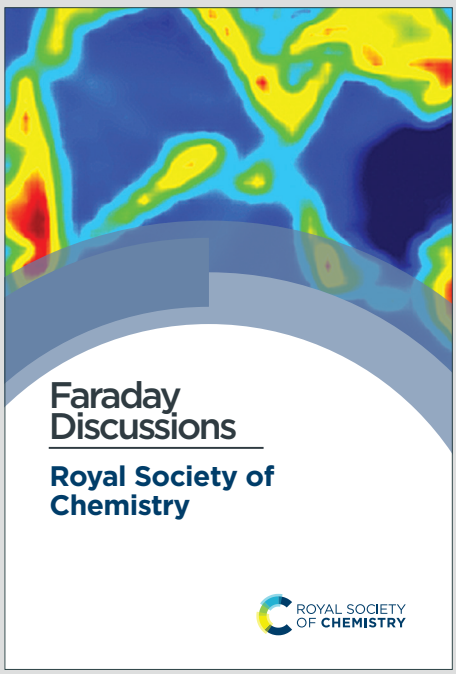

This article can be cited before page numbers have been issued, to do this please use: A. Fauchier-Magnan, L. Trassart, M. Mirolo, A. Rogalev, L. Marchal, A. Bonnet, F. Alloin and C. Villevieille, *Faraday Discuss.*, 2026, DOI: 10.1039/D6FD00037A.

ROYAL SOCIETY OF CHEMISTRY

www.rsc.org/faraday_d

Faraday Discussions

View Article Online
DOI: 10.1039/D6FD00037A

PAPER

Detailed analysis of $Li_6PS_5Cl/LiNi_{0.5}Mn_{0.3}Co_{0.2}O_2$ composite electrode before electrochemical cycling

Adrien Fauchier-Magnan[a,+], Lucas Trassart[a,b+], Marta Mirolo[c], Andrei Rogalev[c], Lauréline Marchal[b], Anthony Bonnet[b], Fannie Alloin[a], Claire Villevieille[a,*]

a. Univ. Grenoble Alpes, Univ. Savoie Mont Blanc, CNRS, Grenoble INP, LEPMI, 38000 Grenoble, France

b. Arkema – Centre de Recherche Rhône-Alpes, Rue Henri Moissan – CS 42063, 69491 Pierre Benite Cedex, France

c. European Synchrotron Radiation Facility (ESRF), CS 40220, 38043, Grenoble Cedex 9, France

Corresponding author: claire.villevieille@grenoble-inp.fr

Received 00th January 20xx, Accepted 00th January 20xx
DOI: 10.1039/x0xx00000x

Solid-state batteries show promise as future energy storage systems. However, reactions between oxide and thiophosphate materials at their interface often cause decomposition, which shortens cycle life. Until now, these interfaces have mainly been studied electrochemically after cell cycling. Nonetheless, ageing may occur while cycling, or even when composite electrodes, blends of electroactive materials and solid electrolytes, are ground together and stored in a glovebox for a week. This paper examines how different storage conditions affect composite electrodes made from $LiNi_{0.5}Mn_{0.3}Co_{0.2}O_2$ (NMC532) paired with Li_6PS_5Cl solid electrolyte. Variables like powder versus pellet form, and storage temperatures at 25°C or 60°C, were evaluated. After just one week, results showed that storing the material as pellets accelerated decomposition due to the close contact between the active material and the electrolyte. Ageing for only one week significantly reduced the specific charge and increased the polarisation during cycling compared to fresh samples. These changes stem from bulk modifications, including the formation of side phases, like transition metal sulfides and LiCl, and surface reactions producing Li_2S. Detailed electrochemical impedance studies revealed that ionic conduction dropped sharply while electronic conductivity rose because of transition metal sulfide formation. The findings highlight how managing electrode ageing is crucial when developing solid-state batteries featuring composite electrodes.

Introduction

Solid-state batteries are widely regarded as a promising next-generation technology for electrochemical energy storage, offering potential advantages such as higher energy density, enhanced safety, and faster charging[1,2]. Despite these benefits, several critical challenges remain, notably the chemical reactivity between key components—including solid electrolytes, electroactive materials, and lithium metal, as well as the optimization of interfaces to ensure efficient ionic and electronic transport. Among currently available solid electrolytes, Li_6PS_5Cl (LPSCl) is considered one of the most promising candidates. It exhibits high room-temperature ionic conductivity (> 2 $mS{\cdot}cm^{-1}$), can be processed and densified without thermal treatment, and is relatively cost-effective[3]. Regarding electroactive materials, layered $LiNi_xMn_yCo_zO_2$ compounds (the NMC family) are particularly attractive due to their high energy density, although excessive nickel content is known to adversely affect electrochemical stability and performance.[4]

In composite positive electrodes, multiple interfaces coexist, most notably those between the active material and the solid electrolyte. Komatsu et al.[5] employed density functional theory (DFT) calculations to investigate the interfacial stability of NMC/LPSCl systems. Their study identified three key parameters governing chemical and electrochemical stability at the NMC/LPSCl interface: the component ratio,

the state of charge (SoC), and the specific NMC composition. In particular, LPSCl was shown to be more reactive with high-nickel-content materials, leading to the formation of Li_3PO_4. Furthermore, they demonstrated that increasing the electrode potential enhances the mutual reactivity between NMC and LPSCl, due to the chemical decomposition of the NMC layer and oxygen release.[6, 7]

View Article Online
DOI: 10.1039/D6FD00037A

Experimental studies have corroborated these theoretical findings. Several groups have reported that contact between LPSCl and NMC523 during cycling leads to the formation of interfacial decomposition products, such as transition metal sulfides (TM_xS_y, where TM = Ni, Co, or Mn)[8-11]. These interphases typically exhibit thicknesses of only a few nanometres. Using electrochemical impedance spectroscopy (EIS), Jung et al.[8] monitored the evolution of interfacial resistance in composite LPSCl/NMC532 electrodes and observed significantly higher resistance in uncoated NMC523, attributed to more extensive decomposition compared with coated materials. Their work also highlighted that chemical degradation occurring in the absence of current can markedly differ from electrochemically induced degradation.

During electrochemical cycling of composite electrodes based on NMC and sulfide electrolytes (LPSCl, LPS (Li_3PS_4) and LGPS ($Li_{10}GeP_2S_{12}$)), the decomposition products commonly include polysulfides, PO_x, and SO_x species[11-15]. The latter two are typically formed at high potentials and are associated with gas evolution, further deteriorating electrochemical performance[16]. It has been demonstrated that decomposition is particularly pronounced because oxygen is supplied solely by the electroactive material, although some uncertainty remains regarding possible contributions from the measurement environment[17, 18]. Notably, the formation of transition metal sulfides locally increases electronic conductivity at the interface, which in turn accelerates the growth of the decomposition layer by facilitating further electrochemical degradation.

From an experimental perspective, Kim et al.[19] examined the interfacial chemistry between LPSCl and both $LiNi_{0.8}Co_{0.1}Mn_{0.1}O_2$ and $LiFePO_4$ during charging and storage at 4.5 V vs. Li^+/Li. X-ray photoelectron spectroscopy (XPS) revealed the formation of NiS at the interface, indicative of sulfur substitution for oxygen in Ni–O bonds. Additionally, significant amounts of PO_4^{3-} species were detected, supporting a mechanism in which O/S exchange contributes to the formation of a cathode–electrolyte interphase (CEI) between the solid electrolyte and the cathode active material (CAM). In a subsequent study, Kim et al.[20] attempted to artificially form a CEI via thermal treatment, producing an interphase composed predominantly of $Li–P–O_x–S_y$ and LiCl. Such an engineered interphase may mitigate parasitic reactions, thereby limiting transition metal dissolution and preserving the structural integrity of the NMC phase.

Overall, the fabrication of composite electrodes for solid-state batteries remains highly challenging due to the complex interplay between chemical and electrochemical reactions, coupled with the demand for high energy density. Achieving this objective requires maximizing the fraction of electroactive material in both weight and volume. However, in composite electrodes, ionic and electronic transport are strongly dependent on composition and interparticle contact. While direct connectivity between NMC particles can ensure sufficient electronic conductivity without additional conductive additives, ionic transport through the solid electrolyte may be hindered by increased tortuosity within the composite[21-23]. Minnmann et al.[24], for example, investigated ionic and electronic conductivities in carbon-free NMC622–LPSCl composites across a range of compositions. They identified two limiting regimes: at low NMC volume fractions, poor electronic percolation isolates active particles and prevents their participation in cycling; at high NMC volume fractions, ionic transport becomes rate-limiting, particularly at high current densities.

Despite extensive research efforts, several challenges remain unresolved for the reliable cycling of composite electrodes in solid-state batteries, among which electrode ageing is of particular importance. Most existing studies focus primarily on electrochemical decomposition processes occurring under applied current. In contrast, the present work provides an in-depth characterization of aged composite electrodes by systematically varying the ageing temperature and the storage configuration, comparing pelletized and powdered forms. Through combined bulk and surface analyses, we demonstrate that the formation of decomposition products—predominantly electronically conductive phases—not only accelerates performance degradation but also severely disrupts ionic transport mechanisms. These effects collectively lead to a pronounced decline in electrochemical performance in aged composite electrodes.

Methods

A Materials

The Li_6PS_5Cl solid electrolyte (referred to as LPSCl) was obtained from NEI Corporation and has particle sizes ranging from 3 to 5 µm. To prevent degradation from exposure to air and moisture, LPSCl is stored in an argon-filled glovebox where both H_2O and O_2 levels are kept below 1 ppm. Polycrystalline NMC532 ($LiNi_{0.5}Mn_{0.3}Co_{0.2}O_2$) was purchased from MTI Corporation and used as the active material. As the theoretical capacity of NMC532 cannot be reached, we used as a benchmark a practical specific capacity of 155 $mAh \cdot g^{-1}$. As lithium metal faces chemical and mechanical problems when contacting thiophosphate electrolytes[25, 26], we used a lithium-indium alloy, prepared by pressing in an argon glovebox an indium disc of 7 mm on a 6 mm lithium disc, both with a thickness of 100 µm. The target composition, $Li_{0.54}In$, provides a stable potential of 0.622 V vs. Li^+/Li.[27]

B Ageing protocol

We assessed the influence of storage conditions on composite electrodes over time using two distinct protocols. Initially, both materials (LPSCl at 25 wt.% and NMC532 at 75 wt.%, corresponding to ca. 46 vol.% and 54 vol.%) were thoroughly mixed by hand for 10 minutes and then subjected to various storage environments. Two hand-mixed NMC/LPSCl powders were stored in powder form at 25°C and 60°C for one week in an argon-filled glovebox. These samples were designated as powder-samples. Additionally, two batches of the mixed powders were first densified at 250 MPa and maintained under a stack pressure of 50 MPa at 25°C and 60°C for one week. These were labelled as pellet-electrodes.

View Article Online
DOI: 10.1039/D6FD00037A

C Electrochemical cell

The experimental setup features a custom electrochemical cell for solid-state batteries and a hydraulic press[28]. The 440C stainless steel cell includes two pistons, a POM disk with O-rings for airtightness, and screws for closure. Pressure is adjustable from 0 to 500 MPa (accuracy: 25 MPa) on a 7 mm diameter cell. Battery components are shaped for 10 minutes at room temperature in an Ar-filled glovebox at 250 MPa and maintained at a stack pressure of 50 MPa[29, 3029, 3029, 3029, 30].

D Electrochemical impedance spectroscopy

Electrochemical impedance spectroscopy (EIS) measurements were performed on a VMP 300 from BioLogic® in an oven for ageing experiments on composite positive electrodes (30 mg). For the electron-blocking system, the experiments were carried out at RT in the glovebox. In the case of ageing, after assembly, the cell was left to rest for 3 hours to reach equilibrium. A perturbation potential of 20 mV was applied at the open-circuit potential over a frequency range between 7 MHz and 100 mHz. The various impedance spectrum treatments (simulation, adjustment) were performed using RelaxIS 3 software.

E Electrochemical cycling protocol

A half-cell, consisting of a solid electrolyte, LiIn negative electrode, and composite positive electrode (aged or fresh), was tested between 3 and 4.3 V vs Li^+/Li at 25°C using a C/20 rate (20h charge/discharge). The loading of active material in the positive composite electrode is between 15 and 16 $mg \cdot cm^{-2}$. The cell is at the OCP for 2 h prior to cycling to ensure thermal stabilization of the cell and the stability of the Li–In alloy. Each charge/discharge included a 60-minute potentiostatic step. Data were collected with a Biologic VMP 300 and analysed using EC-Lab and custom-made Python routines.

F X-ray diffraction

X-ray diffraction (XRD) data were obtained at the ESRF ID31 beamline using a 0.165 Å wavelength and a 0.172 x 0.172 mm^2 beam size. Samples were sealed in 0.7 mm borosilicate glass capillaries for airtightness. Measurements were conducted at room temperature. 2D detector images (Dectris Pilatus CdTe 2M) have been integrated into 1D patterns using the pyFAI package[31] after instrumental calibration using a CeO_2 standard.

G X-ray absorption spectroscopy

X-ray absorption spectroscopy (XAS) was conducted at ESRF on ID12 and BM31 beamlines. K-edges for phosphorus (~2145 eV), sulfur (~2470 eV), and chlorine (~2820 eV) were measured using a custom *ex situ* setup filled in an argon-filled glovebox, collecting only XANES due to their close energies. For NMC532 materials, manganese (~6539 eV), cobalt (~7709 eV), and nickel (~8333 eV) K-edges were recorded in borosilicate capillaries with both X-ray Absorption Near Edge Structure (XANES) and Extended X-ray Absorption Fine Structure (EXAFS) collected.

H X-ray photoelectron spectroscopy

X-ray photoelectron spectroscopy (XPS) signals were obtained using a Thermo Scientific instrument. An Al (Kα) source with an energy of 1486 eV was employed for data acquisition at a grazing incident angle, resulting in a penetration depth of approximately 7 to 10 nm. The XPS analysis was performed using an airtight chamber, facilitating the transfer of samples from the argon glovebox to the XPS device.

Results and Discussion

Solid-state batteries are known to experience long-term cycling stability challenges due to various electro-chemo-mechanical degradation processes. However, to date, there has been no comprehensive investigation into the ageing mechanisms that may arise between thiophosphate-based electrolytes (specifically LPSCl) and electroactive materials such as NMC prior to cycling. Literature suggests the possibility of chemical reactions between sulfur-based and oxide-based components, potentially involving an exchange between sulfur and oxygen[32]. Therefore, we undertook a study to examine the composite electrode in the absence of applied current. Several parameters were selected to evaluate their influence on the ageing of the composite electrode. Firstly, two temperatures were considered: 25°C, and 60°C. Secondly, the storage configuration of the samples (in powder form or as pellets densified at 250 MPa) was studied. Since the study

should reflect the composite electrode used in solid-state batteries, we selected a ratio of 75 wt.% of NMC and 25 wt.% of LPSCl to perform our in-depth structural and chemical investigation.

View Article Online
DOI: 10.1039/D6FD00037A

A Surface analysis of aged powder samples

A mixture containing 25 wt.% LPSCl and 75 wt.% NMC was kept as a blended powder at both 25°C and 60°C for one week. XPS analysis was then performed on the powder samples. **Figure 1** presents the Li1s and S2p core level spectra collected from these samples.

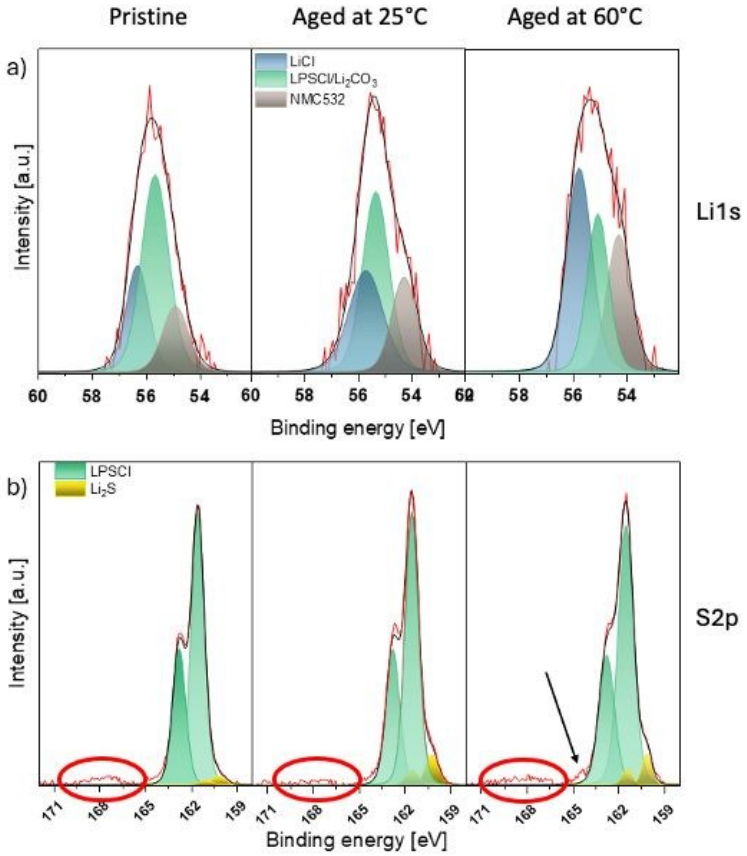

***Figure 1**. a) Li1s and b) S2p core-level spectra performed on the pristine and aged samples. The curves in red are the raw data; the black ones are the envelope obtained from the fitting.*

In XPS core-level spectra, "X"2p signals (where X is P, S, or a transition metal) split into 2p3/2 and 2p1/2 doublets from spin-orbit coupling, with an area ratio of 2:1. The Li1s core-level spectrum of pristine LPSCl/NMC532 mixture (i.e., considered as a "fresh" sample) reveals three peaks assigned to LiCl (56.4 eV), LPSCl/Li_2CO_3 (55.6 eV) and one ascribed to the NMC532 material (54.4 eV) (**Figure 1a)**. The XPS data from NMC532 and LPSCl powders alone are displayed in Supporting Information, **Figure S1**. Based on the data from each pristine material (LPSCl and NMC532), it is difficult to differentiate between the LPSCl and Li_2CO_3 contributions since they have the same binding energy, Li_2CO_3 being a well-known surface product obtained on NMC materials exposed shortly to air (generally at the end of the synthesis)[33]. Since Li_2CO_3 is a surface product, it could easily decompose once in contact with LPSCl (discussion to follow on S2p core level spectrum), leading us to conclude that this contribution is mostly attributed to LPSCl. As can be seen, the storage conditions, in particular the temperature, have an impact on the lithium environment, since the amount of LiCl increases, as well as that of NMC (due to Li_2CO_3 decomposition), showing the decomposition of the solid electrolyte. Furthermore, Li_2S may also be present, but its binding energy can overlap with other contributions.

Regarding the S2p core level spectra presented in **Figure 1b**, several distinctions are observed between the pristine sample and those stored as powders for one week at 25°C and 60°C. The pristine sample exhibits the characteristic signature of LPSCl, with a primary contribution attributed to LPSCl at 161.2 eV and a minor component corresponding to Li_2S at 160.5 eV. At higher binding energies (centred around 168 eV), a slight presence of sulfites and sulfates is apparent, both associated with interactions between NMC532 and LPSCl. Notably, the LPSCl signature alone[6] does not display any indication of sulfite/sulfate species, suggesting that these features may result from reactions involving LPSCl and Li_2CO_3. After one week of storage at 25°C, the S2p core level spectra remain largely unchanged, showing similar contributions; however, an increased amount of Li_2S is detected, indicating partial decomposition of the LPSCl solid electrolyte upon contact with NMC532

powders. For the sample stored at 60°C, an additional contribution is observed at 162.5 eV, highlighted by a black arrow and assigned to P_2S_n and/or Li_2S_n species. This suggests the formation of polysulfides and/or sulfur-bridging species resulting from further decomposition of LPSCl.

View Article Online
DOI: 10.1039/D6FD00037A

Additional analyses were conducted on O1s (**Figure 2**) and Ni2p (**Figure 3**) core-level spectra to investigate the effects of chemical reactions on the NMC532 material. The O1s core level spectrum of pristine NMC532 (**Figure 2**a) reveals three distinct peaks: those at 533.9 and 532.1 eV (green and purple) are likely attributable to the presence of Li_2CO_3, as referenced in previous studies[33], and may originate from the short exposure of NMC532 to air and moisture. Additionally, a contribution at 529.7 eV (blue peak) is observed, corresponding to M–O bonds, where M denotes Ni, Co, or Mn atoms within the NMC532 structure. As the Ni content is higher in the NMC material, we refer to this contribution as Ni-O. For powder samples aged at 25°C (**Figure 2**b), and 60°C (**Figure 2**c), no new features were detected compared to the pristine sample despite an increase in the C-O peak contribution.

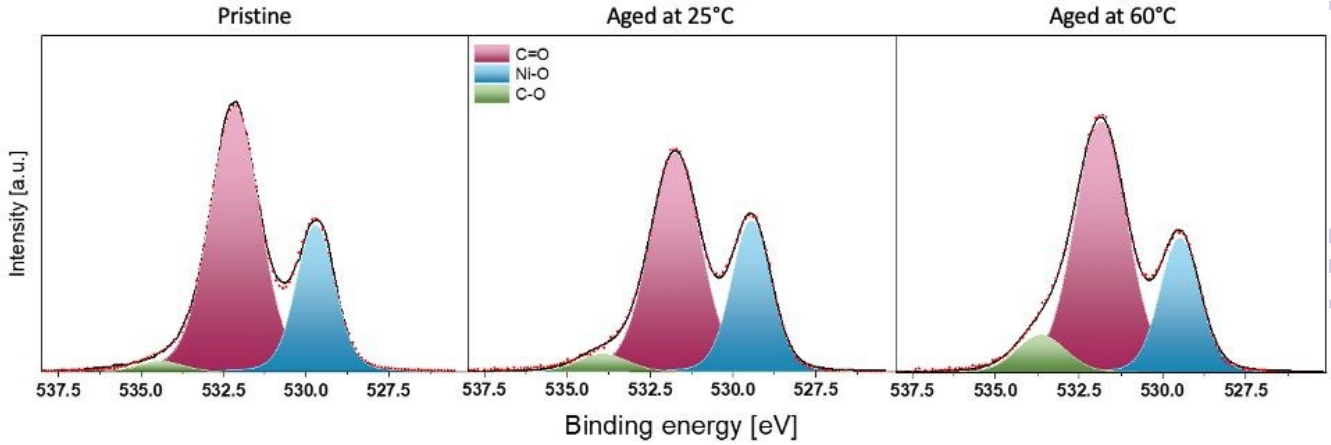

***Figure 2**. O1s core-level spectra for pristine and aged samples.*

Figure 3 presents the data collected at the Ni2p, Co2p and Mn2p core-level energy ranges. It is important to note that the analysis and interpretation of the 2p spectra for 3d transition metals are considerably more complex than those for lighter elements such as P or S. The work of Lu[34] provides a comprehensive discussion of these complexities and elucidates the physico-chemical mechanisms underlying the observed features in the 2p spectra.

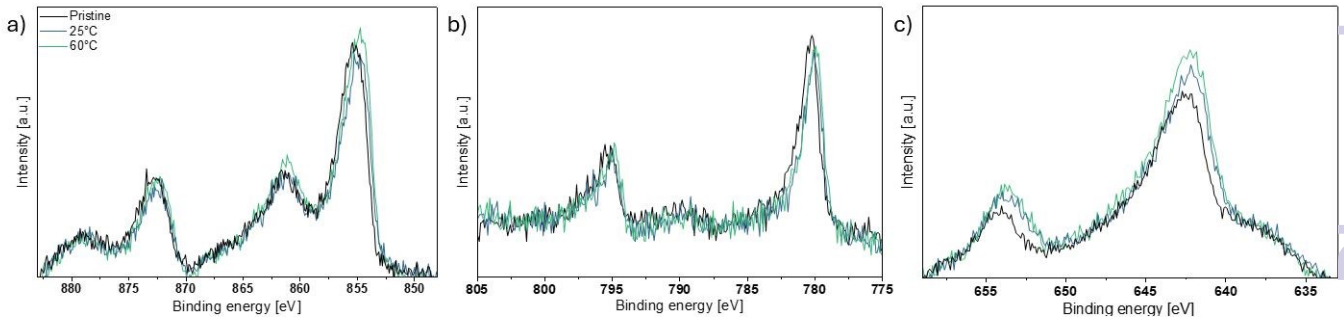

***Figure 3**. a) Ni2p, b) Co2p and c) Mn2p core-level spectra for the NMC532 pristine sample in powder form, and the mixture of LPSCl/NMC532 stored at 25°C and 60°C.*

The Ni2p core level spectrum of pristine NMC532 can be fitted with eight distinct peaks (including the doublets) reflecting the two oxidation states of nickel and the satellite peaks. Specifically, the peaks at 855.2 eV and 872.5 eV correspond to the Ni^{2+} 2p3/2 and 2p1/2 states in NMC (Ni-O), respectively. The presence of Ni^{3+} is attributed to two additional peaks at 856.9 eV and 874.2 eV. For both Ni^{2+} and Ni^{3+}, two satellite doublets are observed at 861.6/878.0 eV and 865.6/879.9 eV, respectively. However, for powder-aged samples, we observe that the overall spectra are shifted to lower binding energy, despite being all calibrated using the peak of C-C at 285 eV. The only reasonable explanation for this feature is a change in the nickel environment like a transition from Ni-O bonds to Ni-S and/or to Ni-O-S bonds, indicating a decomposition of NMC532 once in contact with LPSCl for a prolonged time. The temperature seems to further promote this decomposition as the shift is more pronounced for the same sample stored at 60°C. Based on the work of Maiaugree et al.[35], the peak could be attributed to NiO_xS_y. Similar observations can be seen for Co and Mn elements. These results are in agreement with the XRD investigation discussed later.

After one week, the powders stored at the two different temperatures show a significant signs of chemical reaction between the materials. A similar investigation was conducted on the composite electrode in pellet form, which was densified at 250 MPa for one week, to assess whether enhanced grain-to-grain contact following densification would facilitate decomposition between LPSCl and NMC532.

View Article Online
DOI: 10.1039/D6FD00037A

B Surface characterisation of aged pellets

XPS was conducted on *postmortem* pellet composite-electrode samples after one week of ageing at 25°C and 60°C. We examined the core levels of S2p, and Ni2p—the most chemically and electrochemically sensitive elements in LPSCl and NMC532, respectively. The results for the S2p core level spectra are shown in **Figure 4**.

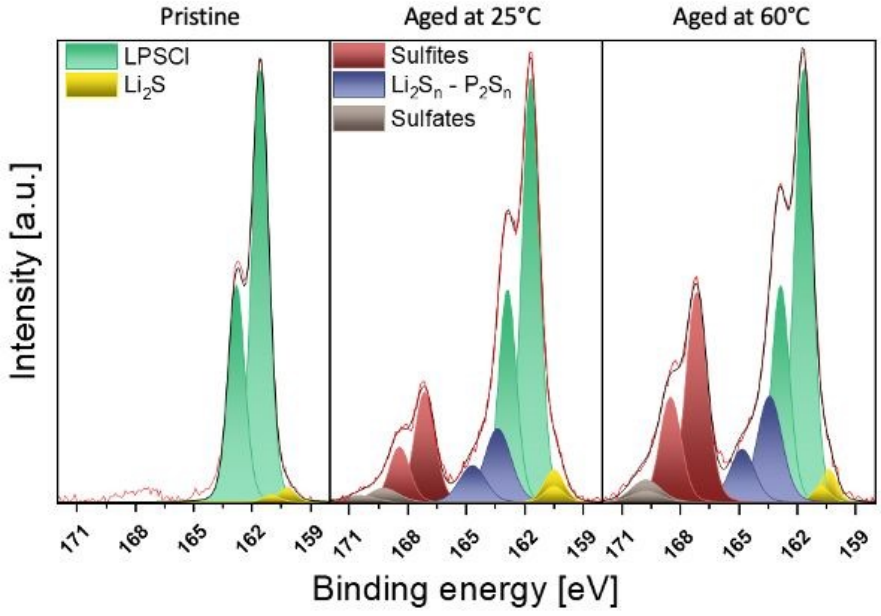

Figure 4. *S2p core-level spectra of LPSCl pristine materials and pellet composite-electrode aged at 25°C and 60°C.*

The two principal contributions observed in pristine LPSCl (**Figure 4,** left)—namely, a doublet at 160.1 and 161.3 eV (Li_2S), alongside another doublet at 161.5 and 162.7 eV (P-S-Li from argyrodite)—are also evident in aged pellet composite samples. In contrast, three additional components are present in the aged samples (**Figure 4** middle and right): the doublet at 162.5 and 164.4 eV assigned to P_2S_m and Li_2S_n, the doublet at 167.1 and 168.4 eV corresponding to sulfites, and the doublet at 169.4 and 170.4 eV linked to sulfates[36]. As the signature of oxysulfur materials such as Ni-O-S can overlap with others, we did not include it in the present spectra. The analysis of the P2p core-level spectra did not reveal any new feature.

We also analysed the Ni2p core-level spectra to assess how ageing affects the NMC material when in contact with the LPSCl solid electrolyte in pellet form (**Figure 5**). The Ni2p core level spectrum of the pristine NMC532/LPSCl mixture displays four contributions, similarly to the samples in powder form: Ni^{2+} at 855.1 and 872.4 eV, and Ni^{3+} at 856.5 and 874.1 eV for the 2p3/2 and 2p1/2 doublets, as well as satellite peaks at 861.5 and 877.3 eV and at 865.7 and 879.8 eV[37]. Aged pellet composite electrode samples show similar features but, once again, the overall spectra are shifted to lower binding energy testifying the presence of at least one extra contribution either from NiO_xS_y (854.2 and 871.4 eV) with a satellite (860.2 and 877 eV) and/or NiS_2.

View Article Online
DOI: 10.1039/D6FD00037A

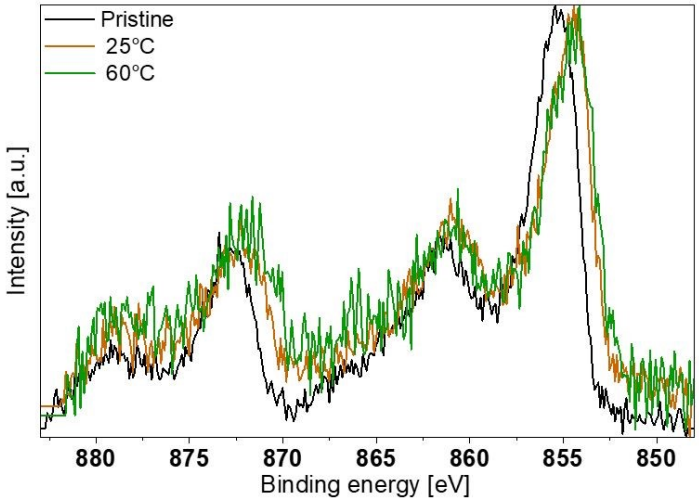

***Figure 5**. XPS Ni2p core-level spectra for NMC pristine and cell-electrode composite aged at 25°C and 60°C.*

The XPS measurements revealed notable changes in surface chemistry upon pellet composite-electrode ageing, with more significant degradation compared to NMC/LPSCl powder mixtures aged at equivalent temperatures. Ageing a densified electrode under pressure enhances the contact between NMC and LPSCl, accelerating interface decomposition into products like sulfate, sulfite, P_2S_m, Li_2S_n, and NiO_xS_y. The formation of these compounds could negatively impact cell performance.

After observing interfacial degradation, we conducted further experiments to assess whether the bulk properties of the material were also affected by the storage conditions. Specifically, high-resolution X-ray diffraction analysis was performed at a synchrotron beamline on the sample stored at 25°C in pellet form.

C Structural characterisation of aged pellets electrode

We performed high-resolution X-ray diffraction on fresh powders and powders aged at 25°C, and Le Bail-type refinement did not show any significant change in the NMC532 lattice parameters between the two samples (**Figure 6**). However, we can still notice some changes, with peaks intensities evolving after ageing, indicating disorder within the NMC532 lamellar structure. Furthermore, the LPSCl signature is barely visible in the aged sample and some secondary phases such as transition metal sulfides can be seen emerging (**Figure 6**, denoted with a *), showing the decomposition of NMC and LPSCl, in agreement with the XPS results. LiCl reflections can also be detected, again indicating the decomposition of LPSCl solid electrolyte. Due to the data quality and the ongoing surface reactions, it was not possible to detect any lattice parameter shift, leading us to conclude that no delithiation of NMC was seen, thus no (Li-ion-based) charge transfer was anticipated between NMC and LPSCl in the aged sample.

View Article Online
DOI: 10.1039/D6FD00037A

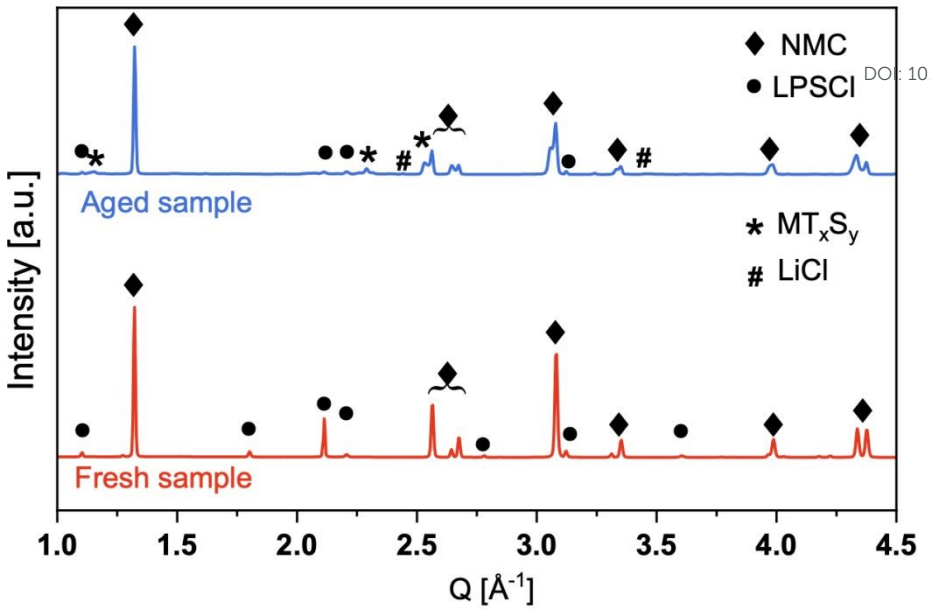

***Figure 6**. X-ray diffractograms acquired in capillaries at the ID31 beamline (ESRF, Grenoble) for the fresh and the aged samples (originally in pellet form, then ground), aged at 25°C.*

Furthermore, X-ray absorption near-edge spectroscopy (XANES) signals were acquired at the K-edge energy level for sulfur, phosphorus and chlorine to check the integrity of LPSCl in the aged sample (pellet aged at 25°C). As can be seen in **Figure 7**, the post-edge of sulfur and chlorine is different for the aged sample, indicating that the environment of the probed atom changed as a function of ageing. For the chlorine K-edge, the aged sample starts to resemble that of LiCl, which fits the observation seen in XRD with the appearance of LiCl reflections. The absorption threshold is also modified with a shift towards higher energies, around 151 eV, which is indicative of greater oxidation of the element (Cl). Almost no modification was noticed for the phosphorus K-edge, meaning that the phosphorus environment remains rather stable.

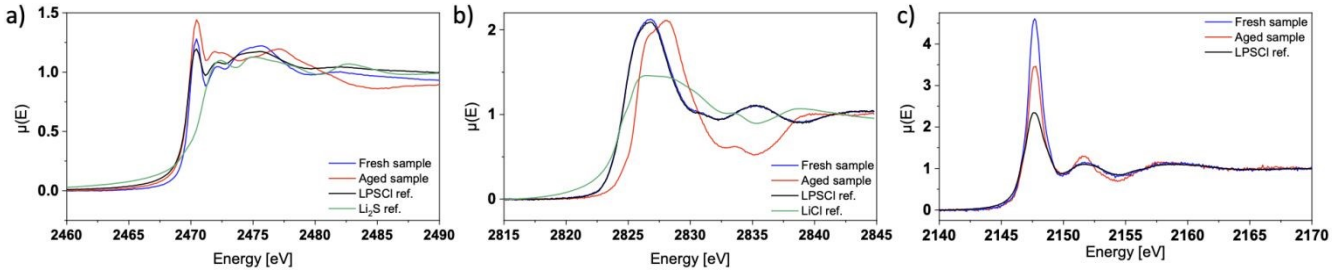

***Figure 7**. XANES spectra at the a) S K-edge, b) Cl K-edge, and c) P K-edge for the aged pellet electrodes at 60°C. Reference samples (Li_2S and LiCl) were also measured as references.*

D Evolution of impedance spectra during ageing on pellet composite electrode

One approach to investigating the chemical reactions occurring within a composite is to analyse its electrochemical impedance response over time, enabling *operando*-type measurements. In this study, we prepared two pellet composite electrodes and monitored their impedance spectra for one week at two distinct temperatures (25°C and 60°C). The primary challenge lies in interpreting the data, as NMC532 exhibits high electronic conductivity while LPSCl serves as an effective ionic conductor. Consequently, both transport phenomena are present in the impedance spectra, making it challenging to attribute specific features to either process. To address this, electrochemical cells were assembled in an "ion-blocking" configuration, with the composite electrode positioned between two current collectors. The literature identifies the transmission line model (TLM) as the most effective approach for modelling transport properties, especially in porous electrode systems.[38, 39] While the traditional TLM works well with liquid electrolytes, it has limitations for solid-state batteries. Jamnik and Maier[40] later introduced a modified TLM tailored for mixed conductors which we slightly modified and used here for our analysis (**Figure S2**).

View Article Online
DOI: 10.1039/D6FD00057A

The Nyquist impedance spectra exhibit pronounced time-dependent evolution as a function of temperature (**Figure 8**). For the pellet composite electrode aged at 25°C, we first observe an increase in the overall system resistance between 8 h and 17 h, followed by a progressive decrease from 17 h up to 138 h, leading to a near short-circuit behaviour. In contrast, for the pellet composite electrode aged at 60°C, the impedance response is similar to a short circuit from the beginning of the measurement, with the total resistance rapidly decreasing before reaching a quasi-stable value.

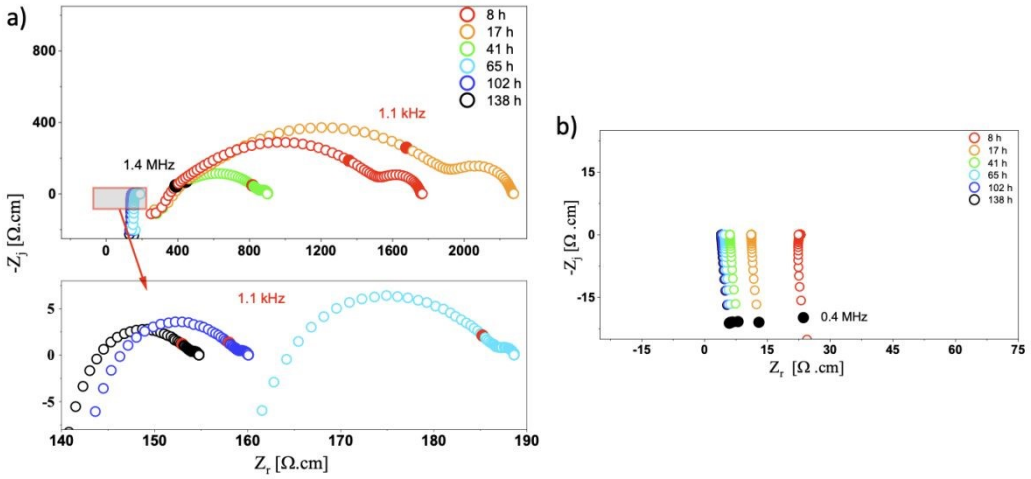

***Figure 8**. Nyquist diagram for a mixture of LPSCl and NMC532 (25%$_{wt.}$ and 75%$_{wt.}$, respectively) aged at a) 25°C and b) 60°C in pellet composite electrode form.*

Without going into too many details about existing models for describing a composite that is a mixed conductor, there are several phenomena that take place. At high frequencies, the impedance response reflects the parallel transport of ions through the LPSCl phase and electrons through NMC–NMC particle contacts. At intermediate frequencies, additional contributions associated with grain boundaries and internal interfaces may become apparent[22]. As the frequency decreases further, ionic motion becomes progressively constrained by the ion-blocking electrodes, leading to ionic charge accumulation and polarization within the composite. This regime is characterized by a Warburg-like response, ideally exhibiting a 45° slope followed by a finite resistance, which corresponds to a finite-length transmission line behaviour[40]. When such a response is observed, the TLM provides an appropriate framework to describe the coupled ionic polarization and electronic conduction in the composite electrode, allowing the effective electronic and ionic conductivity to be extracted. However, when the ionic contribution is not accessible (shunted by the electronic one), the TLM is no longer used, and only the absolute resistance at low frequency (associated with the electronic resistance) is extracted from the fit (**Figure 9**). At 25°C, the ionic conductivity remains stable close to ~0.1 mS·cm^{-1}, during ageing. For the electronic conductivity, after only 8h, it is already lower than that measured for a fresh composite mixture (~ 0.5 mS.cm^{-1} versus ~0.9 mS·cm^{-1}, respectively), but an increase by a factor of 10 of the electronic conductivity is noticed from one day of storage. At 60°C, it is impossible to extract the ionic conductivity, since it is not visible on the impedance spectra.

The initial increase in impedance can be attributed to the formation of degradation products with poorer ionic and/or electronic conductivity, a phenomenon widely reported in the literature and observed in the XPS analysis. Conversely, the subsequent decrease in resistance is more unexpected. It may reflect a reduction in the electronic conduction resistance and/or the onset of a faradaic process. In the former case, this suggests that some degradation products exhibit significant electronic conductivity, as observed for transition metal sulfides (MT_xS_y) found by XPS analyses and XRD data. Additionally, the formation of an interphase at the LPSCl/NMC interface promotes surface oxidation of NMC particles, thereby enhancing their surface electronic conductivity, as well as causing a change in the lithium stoichiometry of NMC which is known to increase its electronic conductivity. Concerning the appearance of faradaic processes between NMC and LPSCl, the fact that no shift in the lattice parameters in the XRD diffractogram is observed for NMC, indicates that this hypothesis is unlikely but could be occurring at the upper surface.

View Article Online
DOI: 10.1039/D6FD00037A

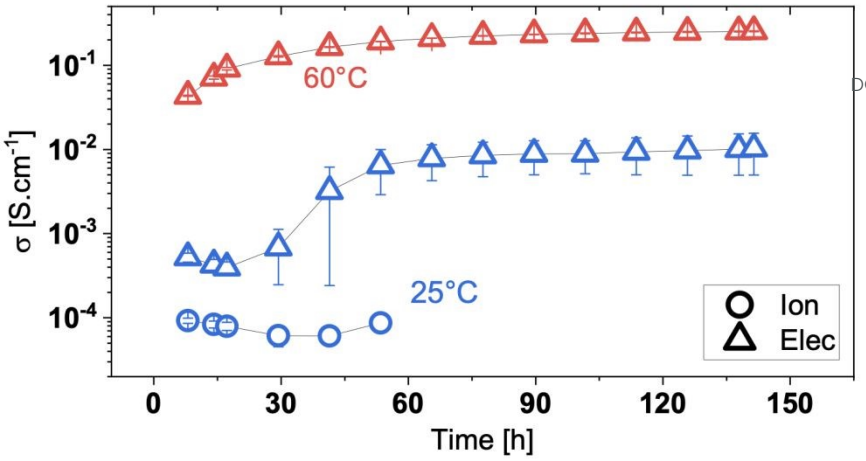

***Figure 9**. Evolution of ionic and electronic conductivities as a function of time for the pellet electrode aged at 25°C and 60°C.*

E Impact of ageing onto ionic transport properties

After one week of ageing in pellet form, the electrochemical cells maintaining the pellet electrode under pressure are opened and assembled in "electron-blocking mode" to evaluate only the composite electrode's ionic transport properties after ageing at 25°C and 60°C (***Figure 10***). In this specific assembly, two layers of solid electrolyte are densified around the composite electrode, then two layers of Li-In are added to prevent low-frequency polarisation. Without the Li-In alloy, blocking behaviour predominates at low frequencies, preventing the extraction of the resistance associated with ionic conductivity (***Figure 10***b).

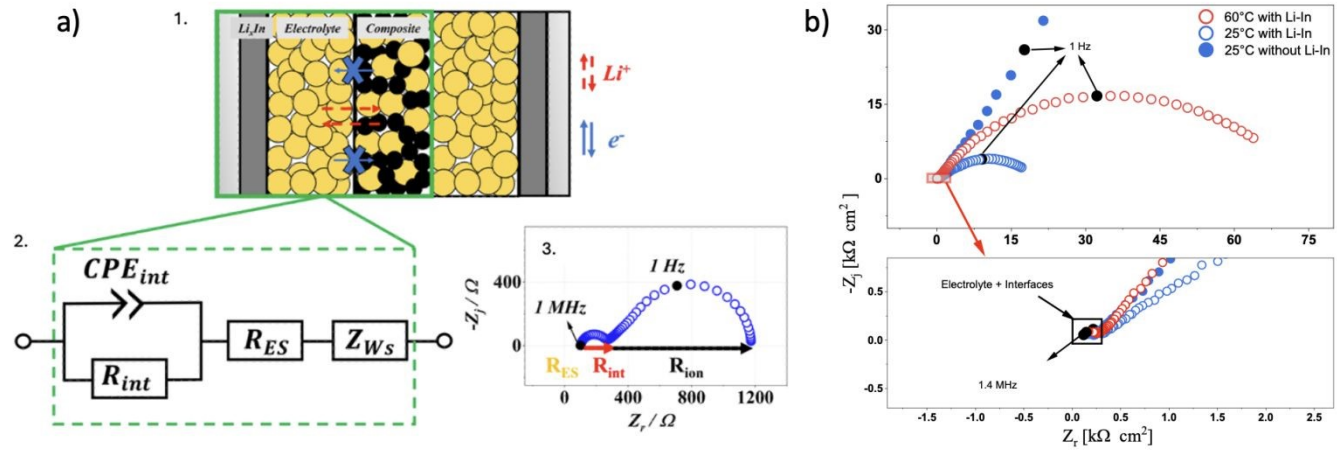

***Figure 10**. a) 1. Scheme of the "electron blocking" configuration and 2. the corresponding equivalent circuit used to analyse the impedance spectrum; 3.) Simulated impedance spectra for "electron blocking" configuration; b) Nyquist diagram obtained in "electron blocking behaviour" for a composite pellet made of a mixture of LPSCl and NMC532 (25%wt. and 75%wt., respectively) aged at 25°C (empty blue circle) and 60°C (empty red circle) measured at room temperature (25°C). For example, a spectrum was acquired before applying the Li-In layers to a mixture aged at 25°C (solid blue).*

When the cell is assembled in an "electron-blocking" configuration (***Figure 10***a), three main contributions can be seen, one at high frequency attributed to the solid electrolyte layer (R_{ES}), one at mid frequency related to interfaces (CPE_{int}//R_{int}), and one at low frequency that exhibits a Warburg-like behaviour followed by a finite resistance, which is characteristic of mixed ionic–electronic conductors under electron-blocking conditions (***Figure 10***b). This response is described by a TLM that accounts for the distributed coupling between ionic polarization and electronic conduction within the composite electrode. However, in the limiting case where the electronic conductivity largely exceeds the ionic conductivity (see below), the low-frequency response of the TLM converges toward that of a finite-length Warburg element. Therefore, for the sake of simplicity and robustness of the fitting procedure, the low-frequency response was modelled using a short Warburg element, which provides an effective representation of the underlying transmission line behaviour.

View Article Online
DOI: 10.1039/D6FD00037A

Knowing the value of the ionic conductivity of the solid electrolyte alone and that of the interfacial processes, it is possible to extract the ionic percolation inside the composite electrode at low frequency (the percolation is hindered due to the porosity of the composite electrode and the dilution of the solid LPSCl matrix). Compared to a fresh composite electrode where the ionic conductivity within the composite electrode was ~10^{-4} S.cm^{-1} at RT, it drops to ~10^{-6} S.cm^{-1} and ~10^{-7} S.cm^{-1} for 25°C and 60°C aged samples, respectively. Furthermore, electronic conductivity is much higher (~10^{-3} S.cm^{-1} - ~10^{-2} S.cm^{-1}) than ionic conductivity for both samples (25°C and 60°C), which justifies the use of the model presented above.

As suspected, the decomposition of the LPSCl solid electrolyte once in contact with the NMC material turns out to be ionically insulating, impacting the electrochemical performance of the cell.

F Aged powder used to assess electrochemical performance of aged materials

The cells are assembled and cycled as described in the Methods section. The results obtained from the powder samples are compared with a fresh mixture (just prepared before cell assembly), both assembled the same day. For the fresh sample, a significant capacity loss is observed during the first cycle between charge and discharge (**Figure 11a**), with the capacity decreasing from approximately 160 to 110 mAh·g^{-1}. This behaviour is consistent with the literature data, and it is due to several decomposition processes[41]. For the samples aged for one week, a significant loss of specific capacity is also observed between the first charge and the first discharge (**Figure 11b**), a phenomenon commonly reported since the first charge leads to interface formation and parasitic reactions between LPSCl and NMC, thereby consuming lithium; these processes are irreversible. However, in the aged cells, already during the first cycle, we observe a drastic decrease in the specific charge compared to the fresh cell. The losses (50% and 70% for mixtures aged at 25°C and 60°C, respectively) are very high compared to fresh sample (~30%). Moreover, the polarization during cycling follows the order: "fresh" mixture < mixture aged at 25°C < mixture aged at 60°C. This trend is consistent with the ionic conductivity values extracted from the composites prior to cycling.

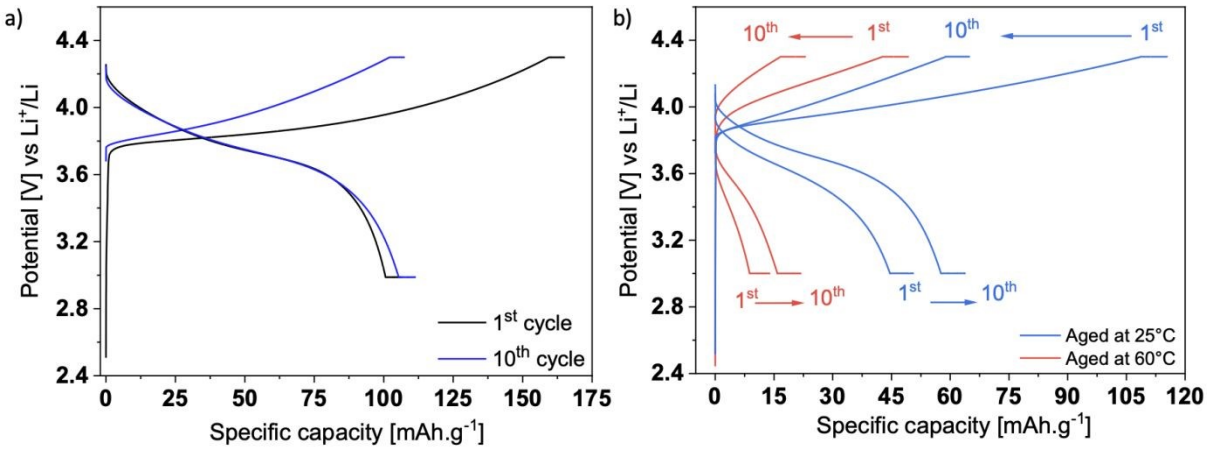

***Figure 11**. Cycling profile of a) the fresh composite electrode (NMC532 and LPSCl) at 25°C, and b) composite electrode performed using aged powder at 25°C and 60°C and cycled at 25°C.*

By plotting the evolution of the specific charge/discharge capacity and the coulombic efficiency (CE) as a function of cycle number, it is possible to estimate the capacity retention after 10 cycles (**Figure 12**). After 10 cycles, the cells with powder mixture aged at 25°C for a week exhibit better capacity retention than those with powder mixtures aged at 60°C (59 ± 8 mAh·g^{-1} and 21 ± 2 mAh·g^{-1}, respectively). The CE also differs between the two mixtures. For the mixture aged at 25°C, after the first cycle, the CE increases relatively rapidly (> 90% by the third cycle) and approaches 100%. In contrast, for the mixture aged at 60°C, the CE takes longer to reach 90% (7th cycle) (**Figure 12a** and **Figure 12b**). This indicates that degradation reactions and/or continuous disconnection of NMC particles from the ionic and/or electronic transport network between charge and discharge are occurring. In comparison, after 10 cycles, the capacity retention for the fresh sample is significantly higher than that of both aged mixtures (100 ± 10 mAh·g^{-1}), and the coulombic efficiency exceeds 95% from the second cycle onward. Consequently, chemical degradation and loss of contact between the solid electrolyte (SE) and NMC532 during cycling are more limited than in the aged mixtures, once again demonstrating that parasitic processes can occur even prior to the onset of battery cycling.

When examining the fraction of capacity arising from the galvanostatic (constant-current) and potentiostatic (constant-voltage) steps, the two aged mixtures exhibit different behaviours, particularly during the galvanostatic step (**Figure 12c** and **Figure 12d**). By contrast, it is rather surprising that the capacity contribution from the potentiostatic step remains identical in all cases. It would have been reasonable to expect the mixture aged at 60°C to access more charge during this step, given its higher initial resistance, but this is not observed. This

suggests that either the interfaces are extremely resistive or that the disconnection of NMC particles is more pronounced in the mixture aged at 60°C than in the mixture aged at 25°C. The latter point aligns well with the decomposition of the electrolyte at 60°C found by structural and chemical data.

View Article Online
DOI: 10.1039/D6FD00037A

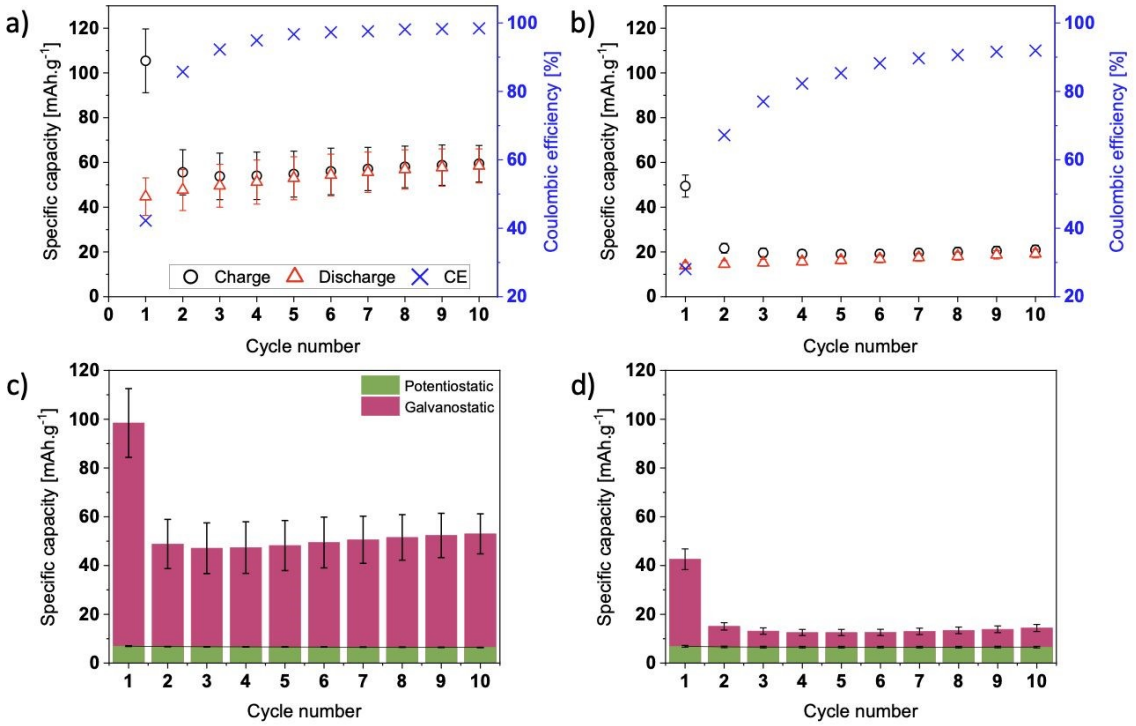

***Figure 12**. Evolution of the specific capacity as a function of the cycle number and the associated coulombic efficiency a) for the sample aged at 25°C and b) for the sample aged at 60°C. Deconvolution of the specific capacity into the specific capacity obtained from the galvanostatic part and that obtained from the potentiostatic part for c) the sample aged at 25°C and, d) the sample aged at 60°C.*

All collected results demonstrate that composite electrodes with powder mixtures aged for even just one week at 25°C exhibit significant signs of degradation, which collectively contribute to the poor electrochemical performance observed.

Conclusions

The electrochemical performance of solid-state batteries often exhibits significant fading, primarily due to electrochemical degradation. In this article, we demonstrate that ageing can occur when powder mixtures or the composite electrodes are prepared and stored in a glovebox for as little as one week at room temperature; the degradation worsens with increasing storage temperature. By assessing several parameters, we determine that storing the electrode in pellet form markedly accelerates surface decomposition, and temperature also impacts the bulk materials. Multiple decomposition products are generated at the interfaces; some of these contain sulfur and oxygen, indicating the degradation of both NMC532 material and LPSCl. Furthermore, these decomposition products substantially affect ionic and electronic transport within the composite electrode, resulting in diminished rate capability and overall electrochemical performance. The combination of advanced characterization techniques enables us to identify and understand the decomposition processes occurring during electrode material ageing, highlighting another crucial parameter to control when assembling solid-state batteries.

Data availability

A data availability statement (DAS) is required to be submitted alongside all articles. Please read our full guidance on data availability statements for more details and examples of suitable statements you can use.

Author contributions

Lucas Trassart: Conceptualization, Methodology, Data Curation, Formal analysis, Investigation, Writing – Review & Editing **Adrien Fauchier-Magnan**: Conceptualization, Methodology, Data Curation, Formal analysis, Investigation, Writing – Review & Editing. **Marta Mirolo**: Formal analysis, Resources, Writing - Review & Editing. **Andrei Rogalev**: Formal analysis, Resources, Writing - Review & Editing. **Laureline Marchal**: Supervision, Project Administration, Writing - Review & Editing. **Anthony Bonnet**: Supervision, Project Administration, Writing - Review & Editing. **Fannie: Alloin**: Formal analysis, Investigation, Validation, Supervision, Project Administration, Writing - Review & Editing. **Claire Villevieille**: Conceptualization, Formal analysis, Investigation, Validation, Resources, Supervision, Project Administration, Writing – Original Draft, Visualisation, Funding acquisition

View Article Online
DOI: 10.1039/D6FD00037A

Conflicts of interest

There are no conflicts to declare.

Acknowledgements

The authors are grateful to Arkema for the financial support of the thesis of Lucas Trassart through a Cifre PhD thesis.
Beamtime at the ESRF was made available through the Battery Pilot Hub MA4929: "Multi-scale Multi-techniques Investigations of Li-ion Batteries: Towards a European Battery Hub". This research has benefited from the characterization equipment of the Grenoble INP–CMTC platform supported by the Centre of Excellence of Multifunctionnal Architectured Materials “CEMAM” (grant ANR-10-LABX-44−01) funded by “Investments for the Future Program.

Notes and references

+ Both authors contribute equally to the study.

1. J. Janek and W. G. Zeier, *Nature Energy*, 2016, **1**, 16141.
2. J. Janek and W. G. Zeier, *Nature Energy*, 2023, **8**, 230-240.
3. R. P. Rao and S. Adams, *physica status solidi (a)*, 2011, **208**, 1804-1807.
4. Y. Kato, S. Shiotani, K. Morita, K. Suzuki, M. Hirayama and R. Kanno, *The Journal of Physical Chemistry Letters*, 2018, **9**, 607-613.
5. H. Komatsu, S. Banerjee, M. L. Holekevi Chandrappa, J. Qi, B. Radhakrishnan, S. Kuwata, K. Sakamoto and S. P. Ong, *The Journal of Physical Chemistry C*, 2022, **126**, 17482-17489.
6. J. Auvergniot, A. Cassel, D. Foix, V. Viallet, V. Seznec and R. Dedryvère, *Solid State Ionics*, 2017, **300**, 78-85.
7. J. Auvergniot, A. Cassel, J.-B. Ledeuil, V. Viallet, V. Seznec and R. Dedryvère, *Chemistry of Materials*, 2017, **29**, 3883-3890.
8. S.-K. Jung, H. Gwon, S.-S. Lee, H. Kim, J. C. Lee, J. G. Chung, S. Y. Park, Y. Aihara and D. Im, *Journal of Materials Chemistry A*, 2019, **7**, 22967-22976.
9. A. Banerjee, H. Tang, X. Wang, J.-H. Cheng, H. Nguyen, M. Zhang, D. H. S. Tan, T. A. Wynn, E. A. Wu, J.-M. Doux, T. Wu, L. Ma, G. E. Sterbinsky, M. S. D’Souza, S. P. Ong and Y. S. Meng, *ACS Applied Materials & Interfaces*, 2019, **11**, 43138-43145.
10. F. Walther, R. Koerver, T. Fuchs, S. Ohno, J. Sann, M. Rohnke, W. G. Zeier and J. Janek, *Chemistry of Materials*, 2019, **31**, 3745-3755.
11. F. Walther, S. Randau, Y. Schneider, J. Sann, M. Rohnke, F. H. Richter, W. G. Zeier and J. Janek, *Chemistry of Materials*, 2020, **32**, 6123-6136.
12. A. Banerjee, X. Wang, C. Fang, E. A. Wu and Y. S. Meng, *Chemical Reviews*, 2020, **120**, 6878-6933.
13. X. Hu, Z. Zhao, Y. Zhao, X. Wang, S. Sainio, D. Nordlund, C. M. Ruse, X.-D. Zhou, S. W. Boettcher, D. Hou, Q.-J. Hong and L. Mu, *Journal of Materials Chemistry A*, 2024, **12**, 3700-3710.
14. R. Fang, Y. Liu, Y. Li, A. Manthiram and J. B. Goodenough, *Materials Today*, 2023, **64**, 52-60.
15. D. Cao, Y. Zhang, A. M. Nolan, X. Sun, C. Liu, J. Sheng, Y. Mo, Y. Wang and H. Zhu, *Nano Letters*, 2020, **20**, 1483-1490.
16. T.-T. Zuo, R. Rueß, R. Pan, F. Walther, M. Rohnke, S. Hori, R. Kanno, D. Schröder and J. Janek, *Nature Communications*, 2021, **12**, 6669.
17. X. Wu, C. Villevieille, P. Novak and M. El Kazzi, *Physical Chemistry Chemical Physics*, 2018, **20**, 11123-11129.
18. X. Wu, C. Villevieille, P. Novák and M. El Kazzi, *Journal of Materials Chemistry A*, 2020, **8**, 5138-5146.
19. T. Kim, K. Kim, S. Lee, G. Song, M. S. Jung and K. T. Lee, *Chemistry of Materials*, 2022, **34**, 9159-9171.
20. J. Kim, S. Lee, H. Lee, J. Park, J. Lee, J. Park, J. Kim, J. Kwon, J. Jin, J. Cho, U. Paik and T. Song, *eTransportation*, 2024, **19**, 100306.
21. W. Jiang, X. Zhu, R. Huang, S. Zhao, X. Fan, M. Ling, C. Liang and L. Wang, *Advanced Energy Materials*, 2022, **12**, 2103473.
22. W. Choi, J. H. Ku, Y. Kim, H. Gwon, G. Yoon, D. Yu and J.-S. Kim, *ACS Applied Materials & Interfaces*, 2024, **16**, 26066-26078.
23. P. Minnmann, F. Strauss, A. Bielefeld, R. Ruess, P. Adelhelm, S. Burkhardt, S. L. Dreyer, E. Trevisanello, H. Ehrenberg, T. Brezesinski, F. H. Richter and J. Janek, *Advanced Energy Materials*, 2022, **12**, 2201425.
24. P. Minnmann, L. Quillman, S. Burkhardt, F. H. Richter and J. Janek, *Journal of The Electrochemical Society*, 2021, **168**, 040537.
25. H. M. Chen, C. Maohua and S. Adams, *Physical Chemistry Chemical Physics*, 2015, **17**, 16494-16506.
26. S. Wenzel, S. J. Sedlmaier, C. Dietrich, W. G. Zeier and J. Janek, *Solid State Ionics*, 2018, **318**, 102-112.
27. A. L. Santhosha, L. Medenbach, J. R. Buchheim and P. Adelhelm, *Batteries & Supercaps*, **0**.
28. X. Wu, M. El Kazzi and C. Villevieille, *Journal of Electroceramics*, 2017, **38**, 207-214.

View Article Online
DOI: 10.1039/D6FD00037A

29. J.-M. Doux, Y. Yang, D. H. S. Tan, H. Nguyen, E. A. Wu, X. Wang, A. Banerjee and Y. S. Meng, *Journal of Materials Chemistry A*, 2020, **8**, 5049-5055.
30. C. Hänsel and D. Kundu, *Advanced Materials Interfaces*, 2021, **8**, 2100206.
31. J. Kieffer and J. P. Wright, *Powder Diffraction*, 2013, **28**, S339-S350.
32. S. K. Martha, E. Markevich, V. Burgel, G. Salitra, E. Zinigrad, B. Markovsky, H. Sclar, Z. Pramovich, O. Heik, D. Aurbach, I. Exnar, H. Buqa, T. Drezen, G. Semrau, M. Schmidt, D. Kovacheva and N. Saliyski, *Journal of Power Sources*, 2009, **189**, 288-296.
33. Y. Bi, T. Wang, M. Liu, R. Du, W. Yang, Z. Liu, Z. Peng, Y. Liu, D. Wang and X. Sun, *RSC Advances*, 2016, **6**, 19233-19237.
34. Q. Lu, *ACS Nano*, 2024, **18**, 13973-13982.
35. W. Maiaugree, A. Tangtrakarn, S. Lowpa, N. Ratchapolthavisin and V. Amornkitbamrung, *Electrochimica Acta*, 2015, **174**, 955-962.
36. P. Naillou, A. Boulineau, E. De Vito, E. Lavanant and P. Azaïs, *Energy Storage Materials*, 2025, **75**, 104050.
37. D. Ko and S. Mhin, *Journal*, 2023, **23**, 5380.
38. R. de Levie, *Electrochimica Acta*, 1963, **8**, 751-780.
39. R. de Levie, *Electrochimica Acta*, 1964, **9**, 1231-1245.
40. J. Jamnik and J. Maier, *Journal of The Electrochemical Society*, 1999, **146**, 4183.
41. S. Puls, E. Nazmutdinova, F. Kalyk, H. M. Woolley, J. F. Thomsen, Z. Cheng, A. Fauchier-Magnan, A. Gautam, M. Gockeln, S.-Y. Ham, M. T. Hasan, M.-G. Jeong, D. Hiraoka, J. S. Kim, T. Kutsch, B. Lelotte, P. Minnmann, V. Miß, K. Motohashi, D. L. Nelson, F. Ooms, F. Piccolo, C. Plank, M. Rosner, S. E. Sandoval, E. Schlautmann, R. Schuster, D. Spencer-Jolly, Y. Sun, B. S. Vishnugopi, R. Zhang, H. Zheng, P. Adelhelm, T. Brezesinski, P. G. Bruce, M. Danzer, M. El Kazzi, H. Gasteiger, K. B. Hatzell, A. Hayashi, F. Hippauf, J. Janek, Y. S. Jung, M. T. McDowell, Y. S. Meng, P. P. Mukherjee, S. Ohno, B. Roling, A. Sakuda, J. Schwenzel, X. Sun, C. Villevieille, M. Wagemaker, W. G. Zeier and N. M. Vargas-Barbosa, *Nature Energy*, 2024, **9**, 1310-1320.

- Data for this article, including XPS, EIS, electrochemical data, XAS are all available at NextCloud UGA at https://cloud.univ-grenoble-alpes.fr/DATA.

DOI: 10.1039/D6FD00037A